Supplementary Material for

Broadband mid-infrared plasmon-polaritons in metallic-dielectric interfaces

Flávio H. Feres[1,2*], Dario A. Bahamon[3], Ingrid D. Barcelos[1], João E. Levandoski[1], Andrea Mancini[4], Thiago M. dos Santos[1], Rafael A. Mayer[1,2], Davi H. S. Camargo[5], Carlos C. B. Bufon[5], Adrian Cernescu[6], Stefan A. Maier[4], Raul de O. Freitas[1] and Francisco C. B. Maia[1,*]

1 – Brazilian Synchrotron Light Laboratory (LNLS), Brazilian Center for Research in Energy and Materials (CNPEM), Zip Code 13083-970, Campinas, Sao Paulo, Brazil.

2 - Physics Department, Gleb Wataghin Physics Institute, University of Campinas (Unicamp), 13083-859 Campinas, Sao Paulo, Brazil.

3 – MackGraphe –Graphene and Nanomaterials Research Institute, Mackenzie Presbyterian University, São Paulo -01302-907, Brazil.

4 – Chair in Hybrid Nanosystems, Nanoinstitute Munich, Ludwig-Maximilians-Universität Munich, Königinstrasse 10, 80539 Munich, Germany

5 - Brazilian Laboratory of Nanotechnology (LNNano), Brazilian Center for Research in Energy and Materials (CNPEM), Zip Code 13083-970, Campinas, Sao Paulo, Brazil.

6 - *Attocube systems AG, 85540, Haar-Munich, Germany.*

- Corresponding authors: francisco.maia@lnls.br, flavio.feres@lnls.br

Summary

I. The damped plane wave model

Fig. S1 presents the illumination scheme of the s-SNOM tip probing the hBN/Au/SiO_2 heterostructure near the edge of the Au film. In this case, the excitation induces strong light confinement at the tip apex and the Au edge due to antenna effect. Hence, tip at $\mathbf{x}$ and edge at $\mathbf{x} = \mathbf{0}$ are turned into the optical near-field sources launching polariton waves. It is worthy to remark that only waves reaching the tip are probed, i.e scattered by the tip to the detector. The edge-launched waves (E^e_{SPP} and E^e_{HPhP}) travelling in the $\hat{x}$ direction reach the tip. But the tip-launched waves (E^t_{SPP} and E^t_{HPhP}), propagating in $-\hat{x}$, do not return to the tip since they are not back-reflected by any reflecting feature in our system. Such fact is confirmed by experimental observations showing no evidence of waves with spatial periods of half wavelengths, which would characterize a reflected wave. Therefore, the modelling considers that the near-field light scattered by the tip is a result from the interference among edge-launched polaritons and a non-propagative term (background). It is assumed that these waves are described by damped plane waves as the edge can be seen as a linear launcher composed of multiple sources. Taking in account the SPPs on Au and the HPhPs in the hBN, the resulting optical field is given by

$$\mathrm{E} = \mathrm{A_{HPhP}} e^{-i(q_{HPhP} - i.\gamma_{HPhP})x - i.\theta} + \mathrm{A_{SPP}} e^{-i.(q_{SPP} - i\gamma_{SPP})x} + \mathrm{C} \qquad \text{(Eq. S1)},$$

where the waves are defined by amplitude A_α, momentum q_α and damping γ_α, with α = SPP or HPhP. C is complex non-propagative background and θ, the relative phase difference between the waves. Eq. S1, the same as Eq. 1, is used in the fits.

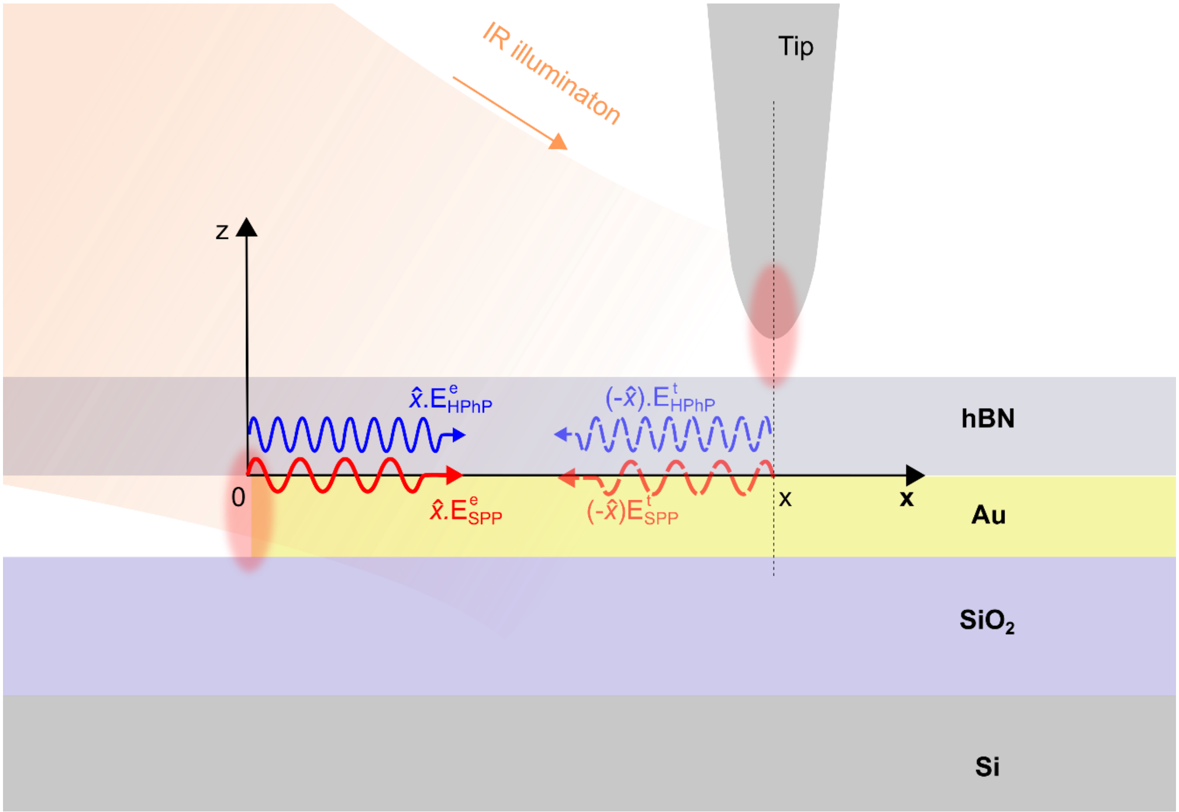

Figure S1 *– Reference frame for the model-fit.*

II. Fourier Transform of profiles of hBN/Au/SiO_2 and Au/SiO_2 images illuminated at ω = 1470 cm^{-1}.

Figure S1 shows the images of hBN/Au/SiO_2 (Fig S1a) and Au/SiO_2 (Fig. S1d) and corresponding profiles and their model-fits (Fig. S1b and S1e). Those figures are the same shown in Fig. 1d-g of the main manuscript. In Fig. S1c and S1f, it is displayed the Fourier Transforms of the profiles in S1b and S1e, respectively. It is observed that peaks corresponding to the SPP and HPhP rise only for P_1' and P_2', thus, validating our choices in the fitting analyses.

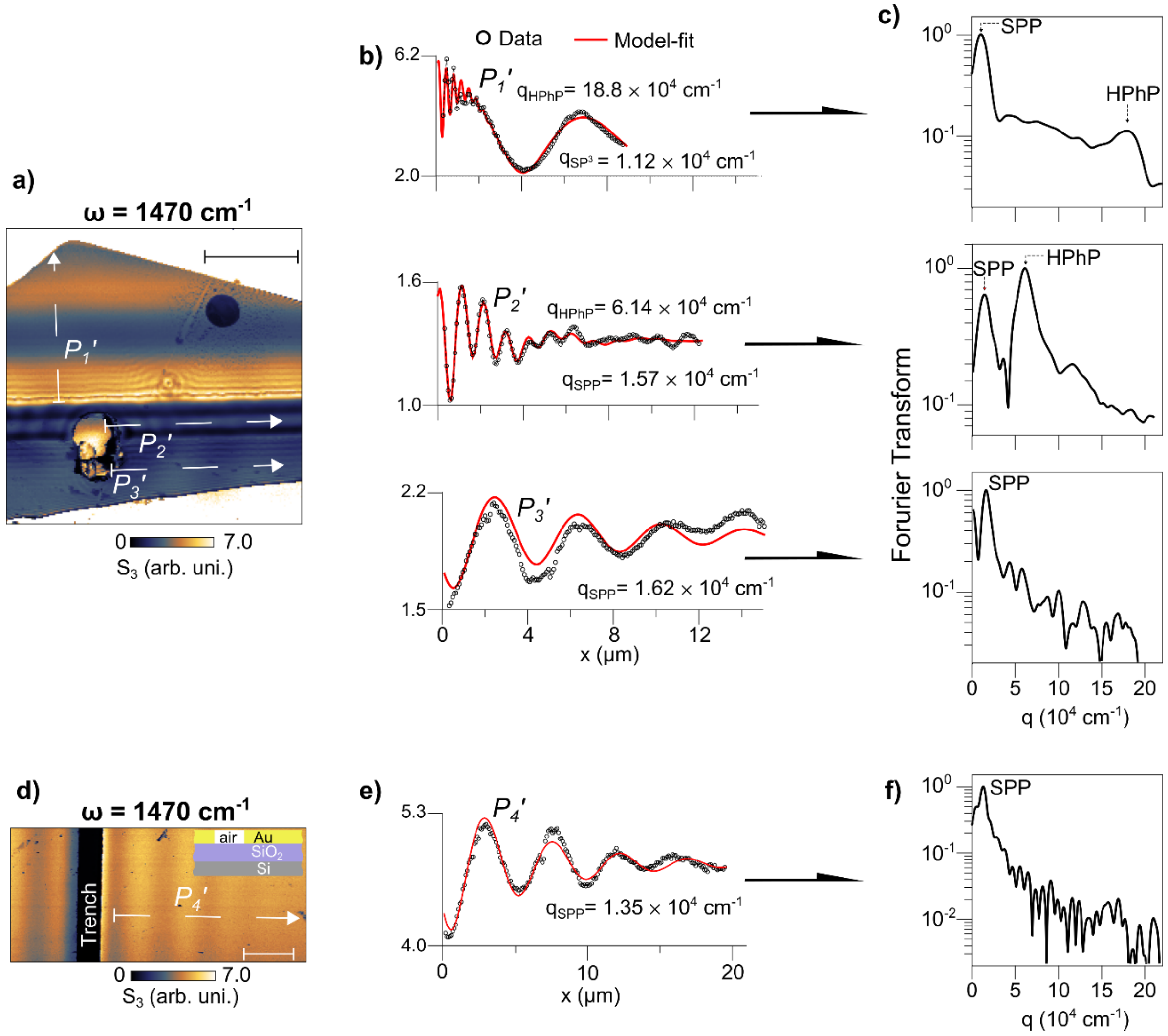

Figure S1 *- Same as in Fig. 1 of the main text:* ***a****) S_3 image of hBN/Au/SiO_2 illuminated at* $\omega = 1470\ cm^{-1}$ *and* ***b****) extracted profiles from (****a****) and corresponding model-fits.* ***c****) Fourier Transform of the profiles in (****b****).* ***d****) S_3 image Au/SiO_2 illuminated at* $\omega = 1470\ cm^{-1}$. ***e****) profile P_4' and the corresponding fit.* ***f****) Fourier Transform of P_4'.*

III. Experimental Dispersion by One-Sided Fourier Transform

The frequency dispersion relation $\omega - \boldsymbol{q_{SSP}}$ plots of the main manuscript are constructed from eq. S2

$$Re[\mathfrak{F}(q,\omega)] = \frac{1}{\sqrt{2\pi}}\left[\frac{q_{SPP}(\omega)}{(q_{SPP} - q)^2 + \gamma_{SPP}^2(\omega)}\right] \qquad (S2)$$

that is the real part of the normalized damped plane wave (eq. S1)

$$\mathrm{E}(x) = \begin{cases} 0 & -\infty < x < 0 \\ e^{-i.(q_{SPP} - i\gamma_{SPP})x} & 0 \leq x < \infty \end{cases} \qquad (S3),$$

which is defined for positives values of position ($0 \leq x < \infty$).

In Figure S2a and S2b we plot Re[E(ω, x)] (Eq. S1) and Re[$\mathfrak{F}(q, \omega)$] (Eq. S2), respectively, using the fit-extracted γ_{SPP} and q_{SPP} as experimental inputs. In comparison, in Figure S2c and S2d the same equations are plotted but using the theoretical values of γ_{SPP} and q_{SPP}, obtained from the multilayer model as inputs. One can see a good correspondence between theory and experiment, thus, corroborating the validity of our analysis.

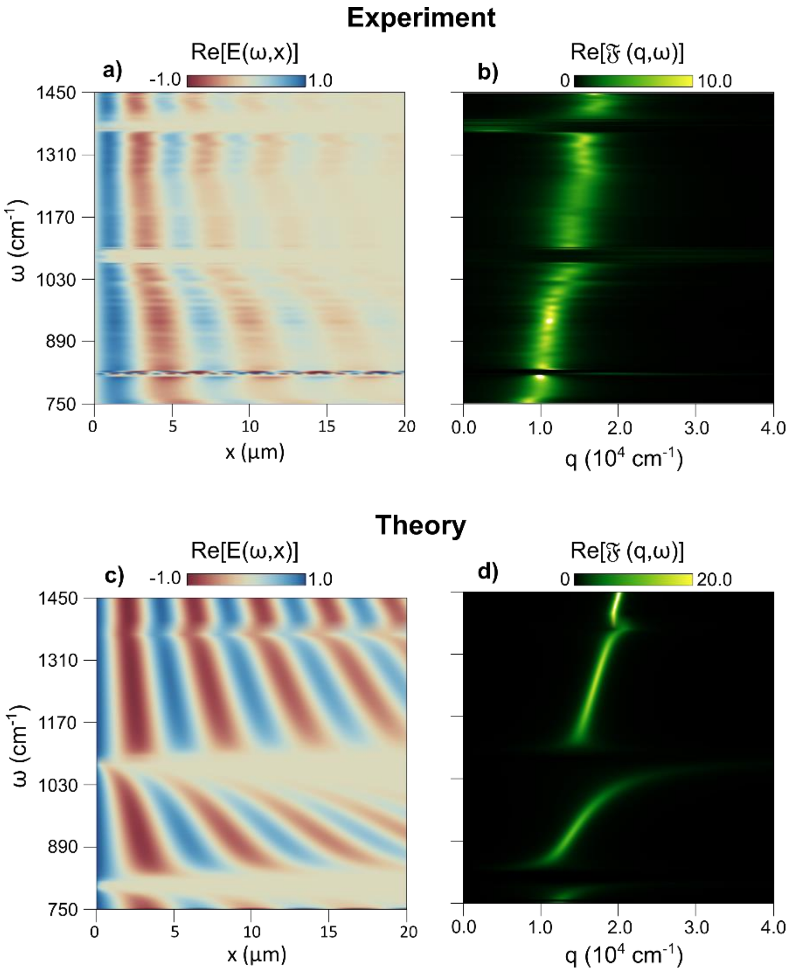

Figure S2 *– a)* Re[$E(\omega, x)$] *and b)* Re[$\mathfrak{F}(q, \omega)$] *using the experimental inputs γ_{SPP} and q_{SPP} extracted from fits. The corresponding plots generated from theoretical values of γ_{SPP} and q_{SPP} are shown in c) and d).*

We also present in Figure S3 the Re[$\mathfrak{F}(q, \omega)$] for different ω's is resonant with the corresponding momentum. It is seen that the damping value modulates the full width at a half maximum of Re[$\mathfrak{F}(q, \omega)$].

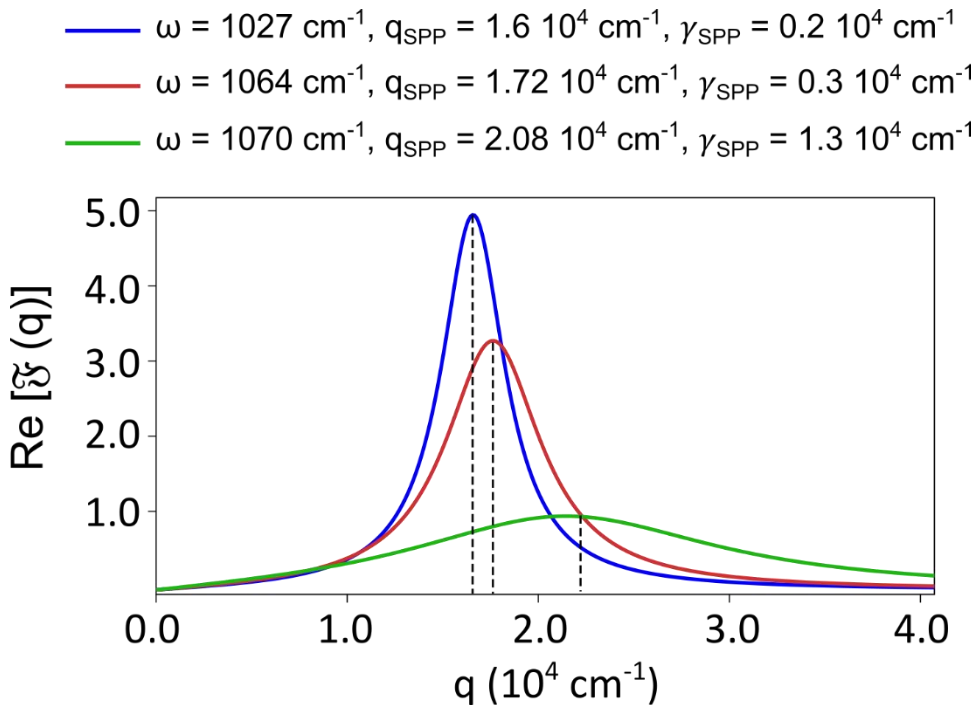

***Figure S3** – Behavior of* $\mathrm{Re}[\mathfrak{F}(q,\omega)]$ *for different values of momentum and damping.*

IV. Coupled Harmonic Oscillators Model

The coupling regime between the SPP waves and the phonons is assessed by the two coupled harmonic oscillators[1–3] model that is characterized by the coupled equations of motion (S4)

$$\begin{cases}\ddot{x}_{SPP}(t) + \Gamma_{SPP}\dot{x}_{SP}(t) + \omega_{SPP}^2 x_{SPP}(t) - \Omega\bar{\varpi}x_{PP}(t) = F_{SPP}(t) \\ \ddot{x}_{PP}(t) + \Gamma_{PP}\dot{x}_{PP}(t) + \omega_{PP}^2 x_{PP}(t) - \Omega\bar{\varpi}x_{SPP}(t) = F_{PP}(t)\end{cases} \quad \text{(S4),}$$

where ω_{SSP}, Γ_{SSP} and x_{SPP} are the frequency, damping and displacement of the SPP modes respectively. The corresponding parameters of the phonons modes are indexed with PP. Ω represents the coupling strength. By definition, $\bar{\varpi} = (\omega_{SP} + \omega_{PP})/2$. F_{PP} and F_{SP} are the effective forces that give energy to the system and are proportional to the external electric field. Considering harmonic time-dependent solutions, $Ae^{-i\omega t}$, equation (S4) can be written as (S5)

$$\begin{cases}(-\omega^2 - i\Gamma_{SPP}\omega + \omega_{SPP}^2)x_{SP} - \Omega\bar{\varpi}x_{PP} = F_{SPP} \\ (-\omega^2 - i\Gamma_{PP}\omega + \omega_{PP}^2)x_{PP} - \Omega\bar{\varpi}x_{SPP} = F_{PP}\end{cases} \quad \text{(S5).}$$

Denoting $\Delta_1 = -\omega^2 - i\Gamma_{SP}\omega + \omega_{SP}^2$, $\Delta_2 = \Omega\bar{\varpi}$ and $\Delta_3 = -\omega^2 - i\Gamma_{PP}\omega + \omega_{PP}^2$, we can rewrite (S5) as following

$$\mathbf{A}\begin{pmatrix} x_{SP} \\ x_{PP}\end{pmatrix} = \begin{pmatrix} F_{SP} \\ F_{PP}\end{pmatrix}; \ \mathbf{A} = \begin{pmatrix} \Delta_1 & -\Delta_2 \\ -\Delta_2 & \Delta_3\end{pmatrix} \quad \text{(S6)}$$

$$\begin{pmatrix} x_{SP} \\ x_{PP} \end{pmatrix} = \mathbf{A}^{-1} \begin{pmatrix} F_{SP} \\ F_{PP} \end{pmatrix} \tag{S7}$$

From (S7), ω_{SP} and ω_{PP} can be easily calculated

$$x_{SP}(t) = \left(\frac{\Delta_3 F_{SP} + \Delta_2 F_{PP}}{\text{Det } \mathbf{A}} \right) e^{-i\omega t} \tag{S8}$$

$$x_{PP}(t) = \left(\frac{\Delta_2 F_{SP} + \Delta_1 F_{PP}}{\text{Det } \mathbf{A}} \right) e^{-i\omega t} \tag{S9}$$

Thus, with the solutions for the equation of motion, we can calculate the extinction coefficient $C_{\text{ext}}(\omega)$, eq. S10, which is proportional to the power loss of the coupling mechanism.

$$C_{\text{ext}}(\omega) \propto \langle F_{PP} \cdot \dot{x}_{PP} + F_{SP} \cdot \dot{x}_{SP} \rangle \tag{S10}$$

$$C_{\text{ext}}(\omega) \propto \ \text{Im}\left[\frac{\Delta_3}{\text{Det } \mathbf{A}}\right] F_{SP}{}^2 \omega + \text{Im}\left[\frac{\Delta_1}{\text{Det } \mathbf{A}}\right] F_{PP}{}^2 \omega + 2\text{Im}\left[\frac{\Delta_2}{\text{Det } \mathbf{A}}\right] F_{PP} F_{SP} \omega \tag{S11}$$

Following the same method of ref. [1], $C_{\text{ext}}(\omega)$ is assumed to be proportional to the $\mathfrak{F}(q, \omega)$ in the iso-momentum regime. Furthermore, using the approximation $F_{SP} \sim F_{PP} \sim 0$, the expressions of ω_{-}^{+} are determined (S12) with Det $\mathbf{A} = 0$.

$$\omega_{-}^{+} = \overline{\omega} \pm \frac{1}{2} \text{Re}\left[\sqrt{4g^2 + \left[\omega_{SP} - \omega_{PP} + i \left(\frac{\Gamma_{SP}}{2} - \frac{\Gamma_{PP}}{2} \right) \right]^2 } \right] \tag{S12}$$

V. Dielectric Functions (h-BN, SiO_2 and Au)

The dispersion curves shown in the main text depend on the electrical permittivities of the materials that have dependence on ω. For h-BN[4,5], $\varepsilon_{xx}^{hBN} (= \varepsilon_{yy}^{hBN})$ and ε_{zz}^{hBN} components are given by eq. S13, with $\rho = xx$ and zz. $\varepsilon_{\rho,\infty}^{hBN}$ is the asymptotic permittivity value for high frequencies and Γ_{ρ}^{hBN} is the dielectric loss. For ε_{zz}^{hBN} in the hBN lower RS band that is resonant with out-of-plane (z direction) phonons, $\omega_{TO}^{zz} = 750\ cm^{-1}$, $\omega_{LO}^{zz} = 820\ cm^{-1}$, $\varepsilon_{\infty}^{zz} = 2.95$ and

$\Gamma_{zz} = 3\, cm^{-1}$. For the hBN upper RS band resonant with in-plane (x direction), $\omega_{TO}^{xx} = 1365\, cm^{-1}$, $\omega_{LO}^{xx} = 1610\, cm^{-1}$, $\varepsilon_{\infty}^{xx} = 4.9$ and $\Gamma_{xx} = 5\, cm^{-1}$[1].

$$\varepsilon_{\rho}^{hBN} = \varepsilon_{\infty}^{\rho}\left(1 + \frac{(\omega_{LO}^{\rho})^2 - (\omega_{TO}^{\rho})^2}{(\omega_{TO}^{\rho})^2 - \omega^2 - i\omega\Gamma_{\rho}}\right) \tag{S13}$$

In the case of SiO_2, the permittivity ε_{SiO_2} is a summation over multiple resonances featuring multiple peaks near ω_1 = 1090 cm^{-1}, ω_1 = 805 cm^{-1} and ω_3 = 457 cm^{-1}. The equation S14 describes the model used, where S_1= 0.452, S_2 = 0.093 and S_3=1.022. Γ_1= 15, Γ_2= 10 and Γ_3= 10 are the crystal dielectric loss of each resonance

$$\varepsilon_{SiO_2} = \varepsilon_{\infty} + \frac{S_1{\omega_1}^2}{{\omega_1}^2 - \omega^2 - i\omega\Gamma_1} + \frac{S_2{\omega_2}^2}{{\omega_2}^2 - \omega^2 - i\omega\Gamma_2} + + \frac{S_3{\omega_3}^2}{{\omega_3}^2 - \omega^2 - i\omega\Gamma_3} \tag{S14}$$

For the metallic media, ε_{Au} follows the Drude model[6,8], where ω_p=8.45 eV/$\hbar$ and $\Gamma_{\mathrm{Au}} = {}^{1}/_{\tau_D}$, with τ_D = 14 ps, are the plasmonic frequency and plasmonic damping, respectively.

$$\varepsilon_{Au} = 1 - \frac{\omega_p^2}{\omega^2 + i\omega\Gamma_{\mathrm{Au}}} \tag{S15}$$

VI. Surface Plasmons Polaritons in Air/Au/SiO_2

In Fig. S4a, it is presented a SINS spectral linescan on Au (90 nm thick) / SiO_2 (2 μm) unveiling the existence of SPP waves (black arrows). In Fig. S4b we show the theoretical $\omega - \boldsymbol{q_{SSP}}$ calculated from the multilayer model[9] for air/Au/SiO_2 (eq. S16). In this equation, $R_j = ik_{jz}/\epsilon_j$ is defined from the *z*-axis momentum $k_{jz} = \sqrt{\epsilon_j k_0^2 - q_{SPP}^2}$ and the in-plane permittivity ϵ_j of each layer *j* (*j* = air, Au and SiO_2) and *a* is the Au thickness. The $\omega - \mathrm{q_{SSP}}$ experimental data (green circles), determined from the model fit as explained in the main manuscript, are also plotted in Fig. S4b. It is noted good agreement between theory and experiment further confirming the generality of the mid-IR SPP waves and our modelling. To compare, we the theoretical dispersion for the Au/SiO_2 interface (white dashed line in Fig. S4b) considering these materials filling the semi-infinity super and substrate (white dashed line shown in Fig S4b).

We note that the AC region near the SiO_2 optical phonons manifests itself either in the theoretical and in the experimental dispersions. The group velocity ($\mathrm{v_g} = \frac{\partial\omega}{\partial q}$) and lifetime ($\tau = \frac{L_x}{\mathrm{v_g}}$) for the modes can be achieved theoretically

(Figure S4 c and S4d). We see that v_g and τ in Au/SiO_2 differ from those in $hBN/Au/SiO_2$ indicating by changing the IMI heterostructure one can also modulate such photonic parameters.

$$\mathbf{det}\begin{vmatrix} e^{ik_{2z}a}(R_1+R_2) & R_1-R_2 \\ R_3-R_2 & e^{ik_{2z}a}(R_3+R_2) \end{vmatrix} = 0 \qquad \text{(S16)}$$

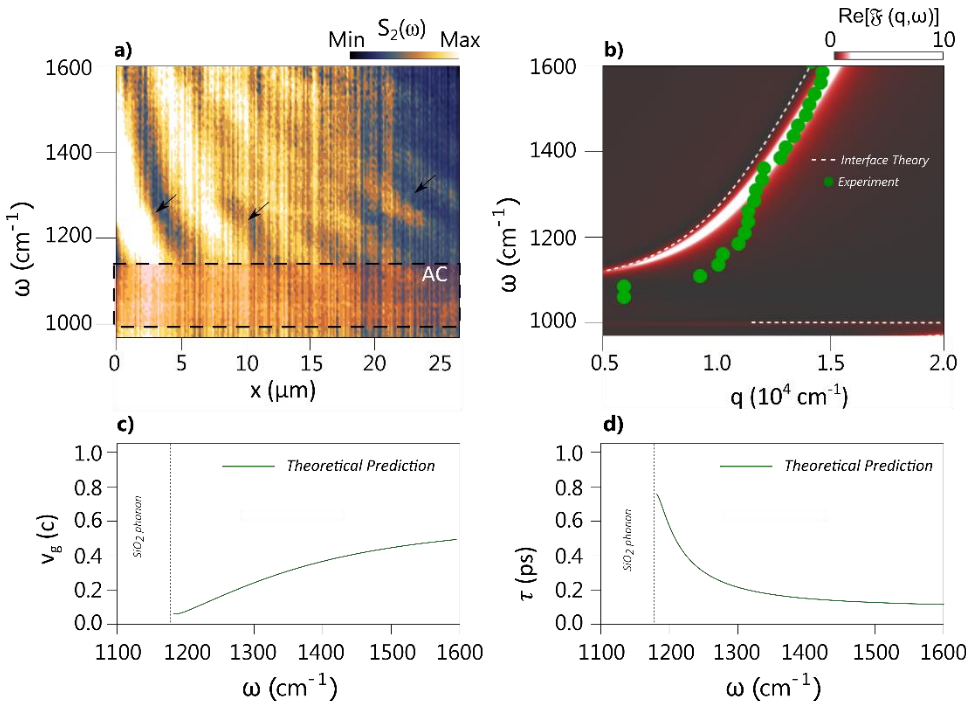

Figure S4- *a) SINS spectral linescan on Au(90 nm)/SiO_2. b) Theroerical $\omega - q_{SSP}$ (map) from eq. S16 and experimental $\omega - q_{SSP}$ (green circles) extracted from the fittings profiles extracted from a). c) and d) theoretical prediciton of v_g and τ for the polaritons modes*

VII. References

1. Bylinkin, A. *et al.* Real-space observation of vibrational strong coupling between propagating phonon polaritons and organic molecules. *Nat. Photonics* 3–9 (2020). doi:10.1038/s41566-020-00725-3

2. Autore, M. *et al.* Boron nitride nanoresonators for phonon-enhanced molecular vibrational spectroscopy at the strong coupling limit. *Light Sci. Appl.* **7**, 17172 (2018).

3. Pons-Valencia, P. *et al.* Launching of hyperbolic phonon-polaritons in h-BN slabs by resonant metal plasmonic antennas. *Nat. Commun.* **10**, 1–8 (2019).

4. Li, P. *et al.* Optical nanoimaging of hyperbolic surface polaritons at the edges of van der Waals materials. *Nano Lett.* **17**, 228–235 (2017).

5. Dai, S. *et al.* Hyperbolic Phonon Polaritons in Suspended Hexagonal Boron Nitride. *Nano Lett.* **19**, 1009–1014 (2019).

6. Feres, F. H., Mayer, R. A., Barcelos, I. D., Freitas, R. O. & Maia, F. C. B. Acceleration of Subwavelength Polaritons by Engineering Dielectric-Metallic Substrates. *ACS Photonics* **7**, 1396–1402 (2020).

7. Yoo, D. *et al.* Ultrastrong plasmon–phonon coupling via epsilon-near-zero nanocavities. *Nat. Photonics* **15**, 125–130 (2021).

8. Steinberger, B. *et al*. Dielectric stripes on gold as surface plasmon waveguides. *Appl. Phys. Lett.* **88**, 1–4 (2006).
9. Maier, S. A. *Plasmonics: Fundamentals and Applications*. (Springer US, 2007). doi:10.1007/0-387-37825-1